The relationship between the statistics of open ocean currents and the temporal correlations of the wind stress

The relationship between the statistics of open ocean currents and the temporal correlations of the wind stress

Golan Bel[1] **and Yosef Ashkenazy**

Department of Solar Energy and Environmental Physics, Blaustein Institutes for Desert Research, Ben-Gurion University of the Negev, Sede Boqer Campus 84990, Israel
E-mail: bel@bgu.ac.il

Abstract. We study the statistics of wind-driven open ocean currents. Using the Ekman layer model for the integrated currents, we investigate analytically and numerically the relationship between the wind-stress distribution and its temporal correlations and the statistics of the open ocean currents. We found that temporally long-range correlated winds result in currents whose statistics is proportional to the wind-stress statistics. On the other hand, short-range correlated winds lead to Gaussian distributions of the current components, regardless of the stationary distribution of the winds, and therefore to a Rayleigh distribution of the current amplitude, if the wind stress is isotropic. We found that the second moment of the current speed exhibits a maximum as a function of the correlation time of the wind stress for a non-zero Coriolis parameter. The results were validated using an oceanic general circulation model.

S Online supplementary data available from stacks.iop.org/NJP/15/053024/mmedia

[1] Author to whom any correspondence should be addressed.

IOP Institute of Physics ⬥ DEUTSCHE PHYSIKALISCHE GESELLSCHAFT

Contents

1. Introduction

Ocean currents are generated by local and remote forces and factors, including winds, tides, buoyancy fluxes and various types of waves. While many studies have investigated the distribution of the wind [1–3], focusing on its relevance to energy production, the distribution of ocean currents has received much less attention [4]. Moreover, currently, there is no accepted theory explaining the observed statistics of surface ocean currents.

Here, we propose a simple physical theory for the distribution of wind-driven ocean currents and its relationship to the spatially variable temporal correlations of the wind (see figure 1). We show that the distribution of wind-driven ocean currents strongly depends on the temporal correlations of the wind—when the wind exhibits long-range temporal correlations, the ocean current statistics is proportional to the wind-stress statistics, while for short-range correlations of the wind, the different components of the current vector follow Gaussian distributions. It was previously reported that the probability density function (PDF) of ocean currents follows the Weibull distribution [4–8] (see section 4.2 for details of the Weibull distribution). We argue that this is not necessarily the case even if the wind-stress magnitude is Weibull distributed.

Oceans play a major and important role in the climate system, and ocean circulation underlies many climate phenomena, from scales of meters to thousands of kilometers and from scales of minutes to decades. The gap in our understanding of ocean current statistics leads to a lack of understanding of the statistics of other related climate variables. Filling in this gap will be useful for many fields: it may help one to predict extreme current events and, thus, it may help one to securely design maritime-associated structures. In light of the increasing efforts to find alternative sources of energy and the idea of using ocean currents as such a source, knowledge of the currents' PDF may help one to better estimate the energy production and to appropriately design ocean current turbines that will withstand even extreme current events. Moreover, knowledge of current statistics and, in particular, its relation to the wind-stress statistics may improve the parametrization of small-scale processes in state-of-the-art general circulation models (GCMs).
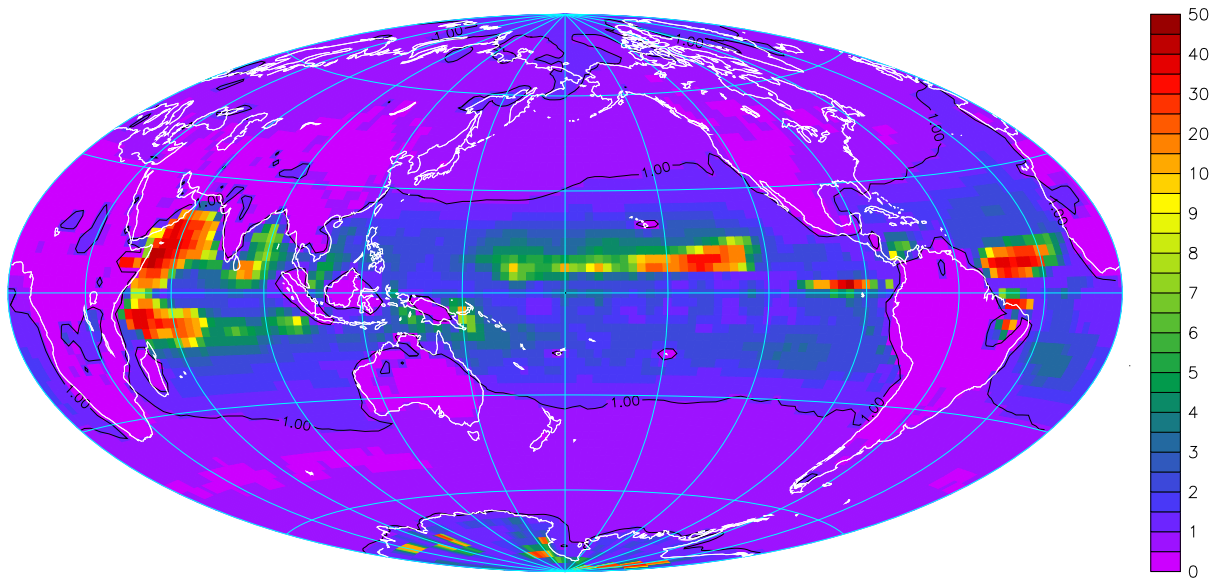
Figure 1. A map of the correlation time (in days) of the wind-stress magnitude. We define the correlation time as the time at which the normalized auto-correlation function first drops below $1/e$. Clearly, there is a large variability in the correlation time. One can also notice the remarkably shorter correlation time over land compared with that over the ocean (except for the polar regions). The map is based on the NCEP/NCAR reanalysis six-hourly wind data for the period of 1993–2010 [27]. The spatial resolution of the data is $2.5° \times 2.5°$. Other definitions of the correlation time yield qualitatively the same results. The black contour line indicates a one-day correlation time, and the white line indicates the coast line. A grid (light blue lines) of $30° \times 30°$ was superimposed on the map.

The study of wind-driven ocean currents goes back more than 100 years to the time when Ekman [9] proposed his classical simple model to explain the effect of the Earth's rotation on upper ocean currents. His model predicted that the depth-integrated current vector is perpendicular to the wind vector, a prediction that was largely proven by observations. Since then, many studies have used Ekman's model to propose more realistic models for ocean currents, as well as for surface winds [10, 11]. In what follows, we use Ekman's model [9] to study the statistics of wind-driven ocean currents.

This paper is organized as follows. In section 2, we describe the Ekman layer model and provide a general (implicit) solution expressed in terms of the characteristics of the wind-stress statistics. In section 3, we consider two idealized cases of wind-stress statistics (step-like temporal behavior of the wind stress in section 3.1 and exponentially decaying temporal wind-stress correlation in section 3.2) and present analytical expressions for the second moment (and the fourth moment for the first case) of the currents' distribution. In section 4, we provide a description of the simple numerical model and of the oceanic GCM (MITgcm) used to validate and extend the analytical results. The numerical tests involve the Weibull distribution; hence, a brief review of the distribution properties and the methods we used to generate correlated and uncorrelated Weibull-distributed time series is provided in section 4.2. The numerical results are presented and discussed in section 5, followed by a brief summary in section 6.

2. The Ekman model

In spite of the simplicity of the Ekman model, it will enable us to start investigating the coupling between the wind stress and the ocean currents. The time, t, and the depth, z, dependent equations of the Ekman model [9], describing the dynamics of the zonal (east–west) U and meridional (south–north) V components of the current vector, are

$$\frac{\partial U}{\partial t} = fV + \nu \frac{\partial^2 U}{\partial z^2},$$
$$\frac{\partial V}{\partial t} = -fU + \nu \frac{\partial^2 V}{\partial z^2}, \tag{1}$$

where $f = (4\pi/T_{\mathrm{d}})\sin(\phi)$ is the local Coriolis parameter (T_{d} is the duration of a day in seconds and ϕ is the latitude), and ν is the eddy parametrized viscosity coefficient, assumed to be depth-independent. In equations (1), we consider $U = \tilde{U} - U_{\mathrm{g}}$ and $V = \tilde{V} - V_{\mathrm{g}}$, where U_{g} and V_{g} are the bottom ocean geostrophic currents determined by the pressure gradient and $\tilde{U}$, $\tilde{V}$ are the actual surface current components. In what follows, we consider the statistics of U and V, where the statistics of $\tilde{U}$ and $\tilde{V}$ can be obtained by a simple transformation. The boundary conditions are chosen such that the current derivative, with respect to the depth coordinate z, is proportional to the integrated current at the bottom of the layer described by our model and to the wind-stress vector (τ_x, τ_y) at the surface [10, 11],

$$\left.\frac{\partial U}{\partial z}\right|_{z=-h} = \frac{r}{\nu}u(t), \quad \left.\frac{\partial U}{\partial z}\right|_{z=0} = \frac{\tau_x}{\rho_0 \nu},$$
$$\left.\frac{\partial V}{\partial z}\right|_{z=-h} = \frac{r}{\nu}v(t), \quad \left.\frac{\partial V}{\partial z}\right|_{z=0} = \frac{\tau_y}{\rho_0 \nu}, \tag{2}$$

where

$$u \equiv \int_{-h}^{0} U(z)\,\mathrm{d}z, \quad v \equiv \int_{-h}^{0} V(z)\,\mathrm{d}z. \tag{3}$$

Here, we introduce the following notation: h is the depth of the upper ocean layer, r is a proportionality constant representing the Rayleigh friction [10, 12–15], (τ_x, τ_y) are the wind-stress components and ρ_0 is the ocean water density (hereafter assumed to be constant, $\rho_0 = 1028\,\mathrm{kg\,m^{-3}}$). The value used for r in the numerical calculations is based on the empirical estimate outlined in [10, 16].

By integrating equations (1) over a sufficiently deep layer (i.e. $h \gg \sqrt{2\nu/|f|}$), we obtain the equations describing the depth integrated currents and their coupling to the wind stress,

$$\frac{\partial u}{\partial t} = fv - ru + \frac{\tau_x}{\rho_0},$$
$$\frac{\partial v}{\partial t} = -fu - rv + \frac{\tau_y}{\rho_0}. \tag{4}$$

In the derivation above, we did not explicitly consider the pressure gradient. Explicit inclusion of the pressure gradient would result in constant geostrophic currents, and equations (4) describe the dynamics of the deviation from the geostrophic currents.

To allow a simpler treatment of these equations, we define $w \equiv u + \mathrm{i}v$. It is easy to show that w obeys the following equation:

$$\frac{\partial w}{\partial t} = -\mathrm{i}fw - rw + \frac{\tau}{\rho_0}, \tag{5}$$

where $\tau \equiv \tau_x + i\tau_y$. Equation (5) is a complex Langevin equation in which the complex noise is not necessarily Gaussian [17]. The formal solution of equation (5) is

$$w(t) = w(0)\, e^{-(if+r)t} + \frac{1}{\rho_0} \int_0^t \tau(t')\, e^{-(if+r)(t-t')}\, dt'. \tag{6}$$

This formal solution demonstrates that the currents depend on the history of the wind stress, and therefore, the distribution of the currents depends not only on the wind-stress distribution, but also on all multi-time moments of the wind stress.

However, the two extreme limits are quite intuitive. When the correlation time of the wind stress, T, is long (i.e. $T \gg 1/r$ and $T \gg 1/f$), one expects that the currents will be proportional to the wind stress since the ocean has enough time to adjust to the wind and to almost reach a steady state. In terms of equation (6), in this limit, $\tau(t')$ can be approximated by $\tau(t)$ since its correlation time is longer than the period over which the exponential kernel is non-zero. In the other limit, when the correlation time of the wind stress is very short (i.e. $T \ll 1/r$ and $T \ll 1/f$), namely, the wind stress is frequently changing in a random way, the ocean is not able to gain any current magnitude. In this case, the central limit theorem [17] implies that each component of the current vector is Gaussian distributed.

It is useful to write the formal expression for the square of the currents amplitude in terms of the wind-stress temporal correlation function. Taking the square of equation (6) and averaging over all realizations (with the same statistical properties) of the wind stress, one obtains

$$\langle |w(t)|^2 \rangle = |w(0)|^2\, e^{-2rt} + \frac{w(0)^*}{\rho_0} e^{-(r-if)t} \int_0^t \langle \tau(t') \rangle\, e^{-(if+r)(t-t')}\, dt'$$

$$+ \frac{w(0)}{\rho_0} e^{-(r+if)t} \int_0^t \langle \tau(t')^* \rangle\, e^{-(r-if)(t-t')}\, dt'$$

$$+ \frac{1}{\rho_0^2} \int_0^t \int_0^t \langle \tau(t')\tau(t'')^* \rangle\, e^{-if(t''-t')}\, e^{-r(2t-t'-t'')}\, dt'\, dt''. \tag{7}$$

The variance of the currents amplitude may be written as

$$\langle |w(t)|^2 \rangle - |\langle w(t) \rangle|^2 = \frac{1}{\rho_0^2} \int_0^t \int_0^t C(t', t'')\, e^{-if(t''-t')}\, e^{-r(2t-t'-t'')}\, dt'\, dt'', \tag{8}$$

where we defined the temporal correlation function of the wind stress as

$$C(t', t'') = \langle \tau(t')\tau(t'')^* \rangle - \langle \tau(t') \rangle \langle \tau(t'')^* \rangle. \tag{9}$$

To allow an analytical treatment, we proceed by considering two special idealized cases in which the formal solution takes a closed analytical form. For simplicity, we only consider the case of statistically isotropic wind stress (the direction of the wind stress is uniformly distributed [18]), namely a case in which the wind-stress components are independent, identically distributed variables with identical temporal autocorrelation functions. The latter assumption is not always valid (see e.g. [19]); however, the generalization of our results to the case of non-isotropic wind stress is straightforward.

3. Idealized cases

3.1. Step-like wind stress

A simple way to model the temporal correlations of the wind is by assuming that the wind vector randomly changes every time period T while remaining constant between the 'jumps'.

By integrating the solution of w (equation (6)) and taking into account the fact that the distribution of w at the initial time and final time should be identical, one can obtain the expressions for the second and fourth moments (ensemble average over many realizations of the stochastic wind stress) of the current amplitude. To better relate our results to the outcome of data analysis, we also need to consider the time average since the records are independent of the constant wind-stress period. The double-averaged second moment of the currents amplitude is defined as

$$\overline{\langle |w|^2 \rangle} \equiv \left\langle \frac{1}{T} \int_0^T |w(t)|^2 \, dt \right\rangle \tag{10}$$

and the angular brackets represent the average over different realizations of the wind stress with the same statistical properties. Using equation (7) and the fact that in this idealized case, the wind stress is constant over the period of the step (T), we obtain for the double-averaged second moment of the currents amplitude (for the details of the derivation see the supplementary material, available from stacks.iop.org/NJP/15/053024/mmedia):

$$\overline{\langle |w|^2 \rangle} = \frac{\langle |\tau|^2 \rangle \left(1 + \frac{1-A_1}{rT} - 2\frac{r(1-A_1)+fA_2}{T(f^2+r^2)}\right)}{(f^2+r^2)\rho_0^2}, \tag{11}$$

where we have introduced the notations $A_1 \equiv \exp(-rT)\cos(fT)$ and $A_2 \equiv \exp(-rT)\sin(fT)$.

The two extreme limits discussed in section 2 can be easily realized and understood. When the correlation time T is very long compared with $1/r$, the second moment of the current is proportional to the second moment of the wind stress, namely, $\langle |w|^2 \rangle = \langle |\tau|^2 \rangle/[(f^2+r^2)\rho_0^2]$. This is exactly what one would expect. The long duration of constant wind stress allows the system to fully respond and adjust to the driving force, and hence, the moments of the currents are proportional to the moments of the wind stress. The coefficient of proportionality is given by the solution of equations (4) with constant wind stress. The other limit is when rT, $fT \ll 1$ and, in this case, $\langle |w|^2 \rangle \sim \langle |\tau|^2 \rangle T/(2r\rho_0^2)$.

In this limit, the second moment of the current amplitude is very small and approaches zero as the correlation time approaches zero. This result is what one would expect for a rapidly changing wind that cannot drive significant currents. Using equation (6) and the fact that wind stress is constant over the step period (T), we calculate the double-averaged (over the step period and the ensemble of wind-stress realizations) fourth moment (for the details of the derivation, see the supplementary material),

$$\overline{\langle |w|^4 \rangle} = \frac{\langle |\tau|^2 \rangle^2 g_2(T) + \langle |\tau|^4 \rangle g_4(T)}{(f^2+r^2)^2 \rho_0^4},$$

$$g_2(T) = \frac{4(D+1-2A_1)}{1-D}\left(\frac{3-D-2A_1 D}{4rT} - 2\frac{3r(1-DA_1)+fDA_2}{(f^2+9r^2)T}\right),$$

$$g_4(T) = 1 + \frac{5-3D+2A_1(A_1-1-D)}{2rT} - 4\frac{3r(1-DA_1)+fDA_2}{(f^2+9r^2)T}$$

$$+ \frac{r(1-A_1^2)+rA_2^2+2fA_1 A_2}{(f^2+r^2)T} - 4\frac{r(1-A_1)+fA_2}{(f^2+r^2)T}, \tag{12}$$

where $D \equiv \exp(-2rT)$. Here, we again use the fact that the integrals of the time averaging are easily carried due to the fact that the wind stress is constant during the averaged period.
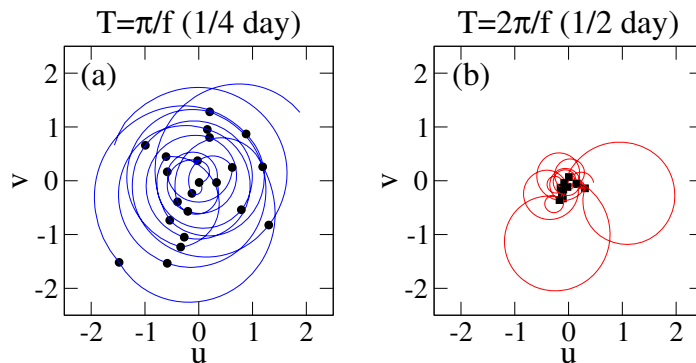
Figure 2. Typical trajectories of the current velocity components for the step-like wind stress. In the left panel, (a) the constant wind-stress duration, $T = \pi/f$, corresponds to changes in the wind stress after the velocity vector completes approximately half a circle. In the right panel, (b), $T = 2\pi/f$, that is, the wind stress changes after a full circle of the velocity field. In both panels, the Coriolis parameter, f, was set to its value at the pole. The symbols indicate the times at which the wind stress was changed.

While at the limit $T \to 0$, both the second and the fourth moments vanish, the ratio between the fourth moment and the square of the second moment remains finite and is equal to 2. This corresponds to the Rayleigh distribution which originates from the facts that the components of the currents are independent and each one has a Gaussian distribution with a zero mean and the same variance.

One can easily understand the origin of the Gaussian distribution by considering the central limit theorem, which can be applied in this limit. Each of the current components is the integral of many independent, identically distributed random variables (the wind stress at different times). Based on the second and fourth moments in the limit of $T \to 0$, we conjecture that the overall PDF of the ocean current speed, in this case, is given by the Rayleigh distribution.

In [20], the case of constant wind stress over some duration was investigated using the depth-dependent Ekman model. The existence of a wind-stress duration for which the current amplitude is maximal was found. The results of this section generalize these results by considering the randomness of the wind stress and its continuity. In addition, we consider here the empirical Rayleigh friction.

In order to better understand the existence of constant wind-stress duration, T, for which the average current amplitude is maximal, we present, in figure 2, two typical trajectories of the current velocity components u, v. The dynamics of the velocity field may be understood as follows. When the friction, r, is smaller than the Coriolis frequency, the velocity field undergoes circular motion and returns, with frequency f, to a point in the velocity space which is very close to the initial point. The initial current is irrelevant since even a small amount of friction ensures that the initial point is close to the origin at the long-time limit. The above dynamics is valid for any value of the temporal wind stress. Therefore, if the wind stress changes with a frequency equal to the Coriolis frequency, the current amplitude cannot be driven far from the origin, and its average remains small (this explains the observed minimum for $T \approx 2\pi/f$). On the other hand, when the wind stress changes with a frequency equal to double the Coriolis
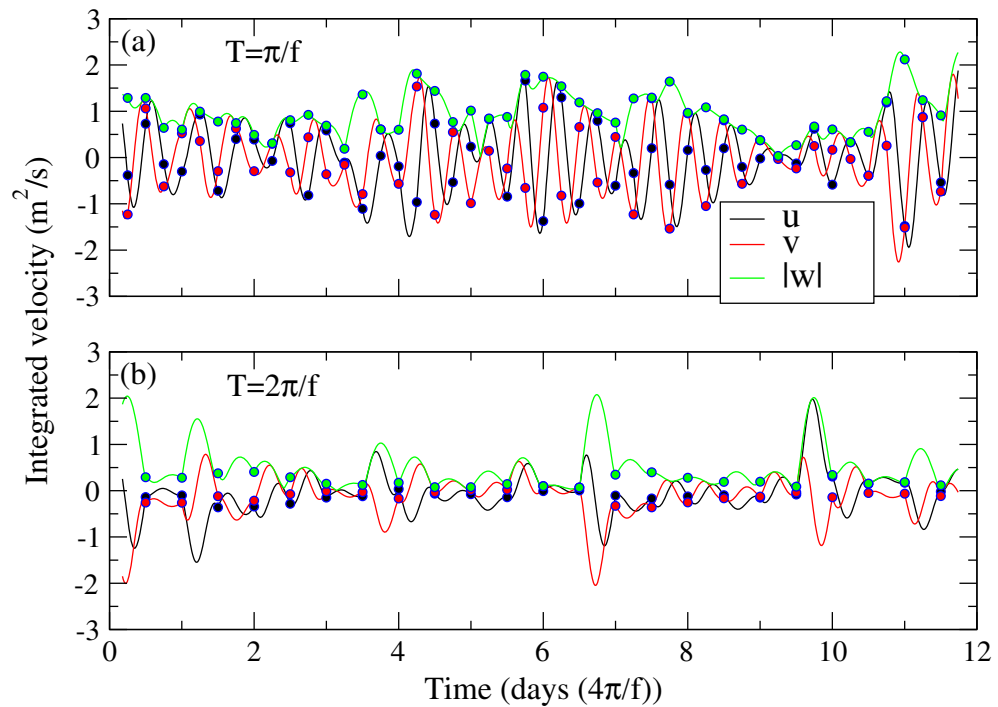
Figure 3. Typical time series of the current velocity components and amplitude. In the top panel, (a), the constant wind-stress duration, $T = \pi/f$. In the bottom panel, (b), $T = 2\pi/f$. In both panels, the Coriolis parameter, f, was set to its value at the pole. The symbols indicate the times at which the wind stress was changed.

frequency, the current velocity reaches the largest amplitude when the wind stress changes and the new circle starts around a different initial point (possibly far from the origin). Therefore, in the latter case, the average current speed is maximal. To better illustrate this picture, we present, in figure 3, typical time series of the current velocity components and amplitude. The dots represent the times when the wind stress changed. It can be seen that for $T = \pi/f$, the typical velocity amplitude when the wind stress changes (the dots in figure 3) is significantly larger than that for $T = 2\pi/f$.

The intuitive explanation above relies on the fact that $r \ll f$. To elucidate the role of the friction, we present, in figure 4, the analytically calculated second moment (equation (11)) of the current versus the constant wind-stress duration for different values of r. When the viscosity is large, there is no maximum but rather a monotonic increase of the average current amplitude as T increases.

3.2. Exponentially decaying temporal correlations of the wind stress

The second case we consider is the Ornstein–Uhlenbeck wind stress. This process results in a Gaussian wind stress with an exponentially decaying temporal correlation function. It is important to note that, due to the Gaussian nature of the force, the first and the second moments of the wind stress, together with its two-point correlation function, provide all the information
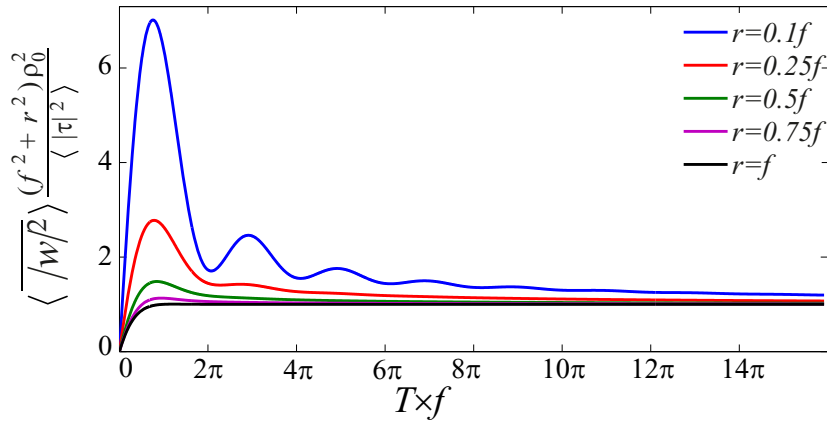
Figure 4. The second moment of the current amplitude (equation (11)) versus the constant wind-stress duration, T. The different lines correspond to different values of the Rayleigh friction, r.

on the driving force. The correlation function of the wind-stress components is given by

$$\langle \tau_i(t)\tau_j(t') \rangle = \delta_{ij}\langle \tau_i^2 \rangle \exp(-\gamma_i|t - t'|). \tag{13}$$

The long-time limits of the current components' averages are

$$\langle u \rangle \sim \frac{r\langle \tau_x \rangle + f\langle \tau_y \rangle}{\rho_0(f^2 + r^2)}, \quad \langle v \rangle \sim \frac{r\langle \tau_y \rangle - f\langle \tau_x \rangle}{\rho_0(f^2 + r^2)}. \tag{14}$$

The long-time limit of the current amplitude variance, $s^2 \equiv \langle |w|^2 \rangle - \langle u \rangle^2 - \langle v \rangle^2$, is given by

$$s^2 \sim \sum_{i=x,y} \frac{\langle \tau_i^2 \rangle (r + \gamma_i)}{\rho_0^2 r(f^2 + (r + \gamma_i)^2)}. \tag{15}$$

Under the assumption of isotropic wind stress, the variance may be expressed as $s^2 \sim \langle |\tau|^2 \rangle (r + \gamma)/(\rho_0^2 r(f^2 + (r + \gamma)^2))$. Note that in deriving the expression above, we assumed that the autocorrelation function of the wind stress is isotropic. In general, this is not the case [19]; however, for simplicity, we present here the results for this special case, and the generalization to the more realistic case is trivial. Due to the Gaussian nature of the wind stress and the linearity of the model, the current components have Gaussian distributions that are fully characterized by the mean and variance. Note that the result of equation (15) holds for any distribution of the wind-stress components, as long as the two-point correlation function is given by equation (13). Equation (15) is easily derived by substituting the two-point correlation function (equation (13)) in equation (8). Similar to the first idealized case discussed above, it is clear that the second moment vanishes at the limit of a short wind-stress correlation time ($\gamma \gg r$ and $\gamma \gg f$).

4. Details of the numerical models

We performed two types of numerical simulations to validate the analytical derivations presented above. The first type was a simple integration of equations (4)—these numerical solutions are provided, both to validate the analytical results and to present the solutions of cases
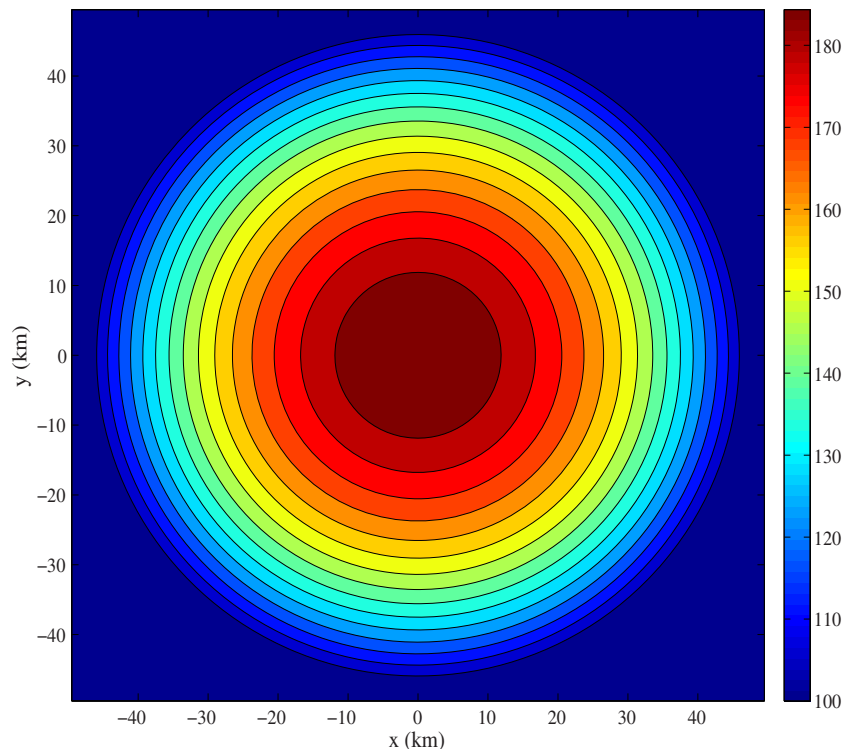
Figure 5. Contour plot of the bathymetry used in the MITgcm simulations.

not covered by the analytical solutions. In the second type of simulation, we used a state-of-the-art oceanic GCM, the MITgcm [21], to test the applicability of our analytical derivations when the spatial variability of the bottom topography and the nonlinearity of the ocean dynamics [10] are taken into account.

4.1. The MITgcm setup and details

The MITgcm solves the primitive equations [21] and is implemented here using Cartesian coordinates with a lateral resolution of 1 km (or 10 km) with 50×50 grid points. We consider open (periodic) and closed physical boundaries of the domain (the results of the closed boundary setup are presented only in the last figure). There is one vertical level that expresses a 2D parabolic basin with a maximum depth of 90 m, as shown in figure 5. The basin is situated in a plateau of 100 m depth. The use of the partial cell option of the MITgcm enables us to handle depth variability, even with a single vertical level. The integration time step is 10 s, and the overall integration time is 2 years. Water temperature and salinity are kept constant. The horizontal viscosity is $1 \, \mathrm{m^2 \, s^{-1}}$ and the vertical one is $1 \times 10^{-4} \, \mathrm{m^2 \, s^{-1}}$. We use the linear bottom drag option of the MITgcm, and the effective drag coefficient is depth dependent where the mean bottom drag coefficient is $1 \times 10^{-5} \, \mathrm{s^{-1}}$. We also use the implicit free surface scheme of the MITgcm.

There are different ways to introduce heterogeneity into the water flow: for example, by forcing the water surface with spatially variable wind stress. Changes in density due to changes in temperature and salinity, as a result of spatially and temporally variable surface heat and
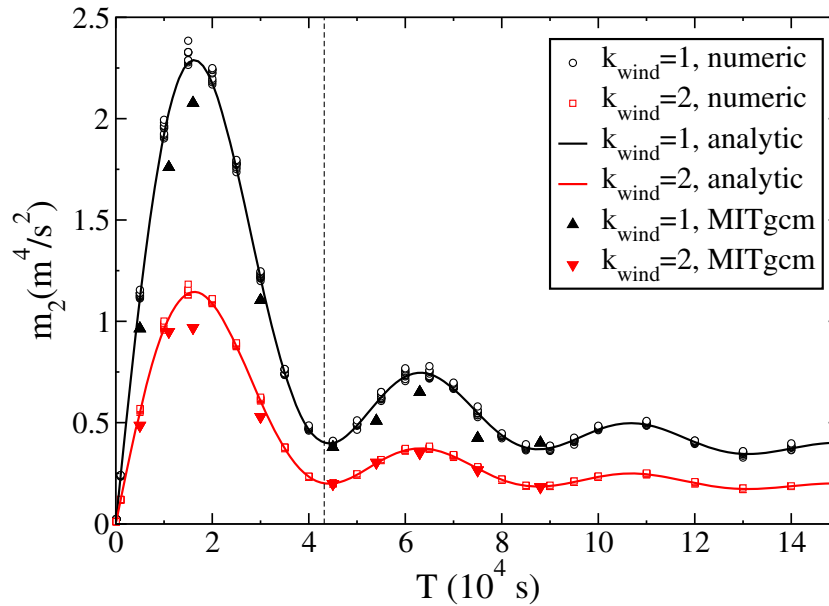
Figure 6. The second moment of the current amplitude versus the constant wind-stress duration, T. The analytical results (solid lines) are compared with the numerical solution of the Ekman model (empty symbols) and with the MITgcm modeling of the currents in a simple artificial lake with open boundaries using a 1 km resolution. The wind-stress amplitude was drawn from a Weibull distribution with two different values of the k_{wind} parameter as specified in the figure. The Coriolis frequency, $f \approx 1.45 \times 10^{-4}\,\text{s}^{-1}$, was set to its value in the pole, and the constant wind duration associated with this Coriolis frequency is indicated by the vertical dashed line. The Rayleigh friction parameter is $r = 10^{-5}\,\text{s}^{-1}$.

freshwater fluxes, can also enrich water dynamics. The main goal of the MITgcm numerical experiments presented here is to validate the analytical results presented above when advection and horizontal viscosity are taken into account. To enrich water dynamics, we chose to vary the water depth when including (excluding) the boundaries of the domain—there is no particular reason for choosing this way over another. We find the depth variability to be simpler, from a numerical point of view, but still rich enough to allow us to study the boundary effects on the water dynamics and to compare the numerical results with the derived analytical expressions.

4.2. The Weibull distribution

It is widely accepted that the PDF of ocean currents follows the Weibull distribution [4–8]; therefore, we use this distribution in our numerical tests. For consistency, we provide here a brief review of its properties and the methods we used to implement temporally correlated and uncorrelated time series. The Weibull PDF is defined for positive values of the variable, $x > 0$, and is characterized by two parameters, k and λ:

$$W_{k,\lambda}(x) = \frac{k}{\lambda}\left(\frac{x}{\lambda}\right)^{k-1}\exp(-(x/\lambda)^k), \tag{16}$$
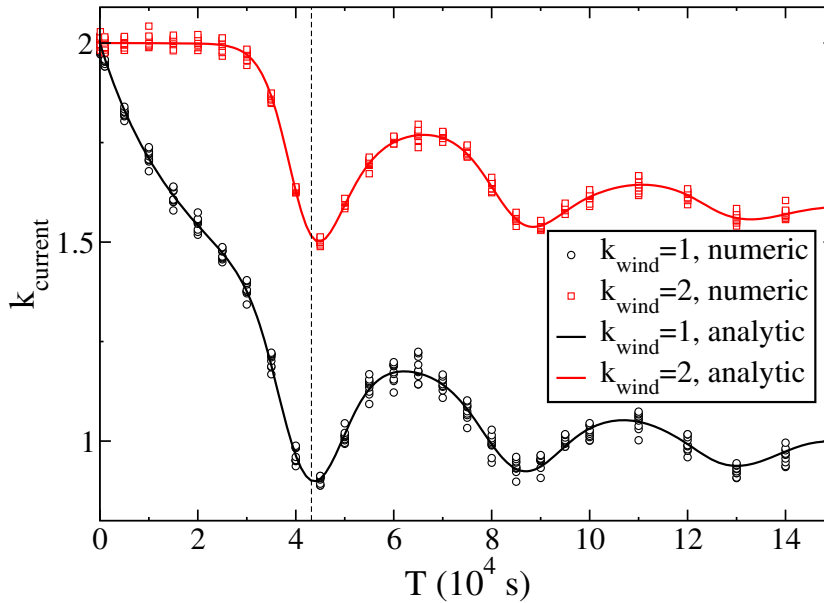
Figure 7. The Weibull $k_{current}$ parameter of the current distribution versus the constant wind-stress duration, T. The analytical results (solid lines) are compared with the numerical solution of the Ekman model (empty symbols). The wind stress was drawn from a Weibull distribution with two different values of the k_{wind} parameter as specified in the figure. The Coriolis frequency, f, was set to its value in the pole and the corresponding duration is indicated by the vertical dashed line.

where λ and k are both positive. λ and k are usually referred to as the scale and shape parameters of the distribution. The cumulative Weibull distribution function is given by

$$F_{k,\lambda}(x) = 1 - e^{-(x/\lambda)^k}. \tag{17}$$

It is possible to express the moments of the Weibull distribution, $\langle x^m \rangle$, using k and λ:

$$\langle x^m \rangle = \lambda^m \Gamma\left(1 + \frac{m}{k}\right), \tag{18}$$

where Γ is the Gamma function. Thus, it is sufficient to calculate the first and second moments of a time series and, from them, to find the k and λ that characterize the Weibull distribution (assuming that we have *a priori* knowledge that the series is Weibull distributed). The k parameter can be calculated using two different moments (n, m) of the time series by solving (numerically) a transcendental equation $\langle x^n \rangle^{m/n} / \langle x^m \rangle = (\Gamma(1 + n/k))^{m/n} / \Gamma(1 + m/k)$, and λ can be estimated by using the first moment (the mean) and the estimated k. It is also possible to calculate the k parameter from the slope of the hazard function of the Weibull distribution $W(x)/(1 - F(x)) = (k/\lambda)(x/\lambda)^{k-1}$ when a log–log plot is used. In this paper, we use the second and fourth moments to derive the values of k and λ. Previous studies used other approximations to estimate k and λ [2, 4].

A special case of the Weibull distribution, called the Rayleigh distribution, is obtained when $k = 2$. It can be associated with the distribution of the magnitude of a vector whose components are two independent, Gaussian-distributed, random variables; that is, if x and y
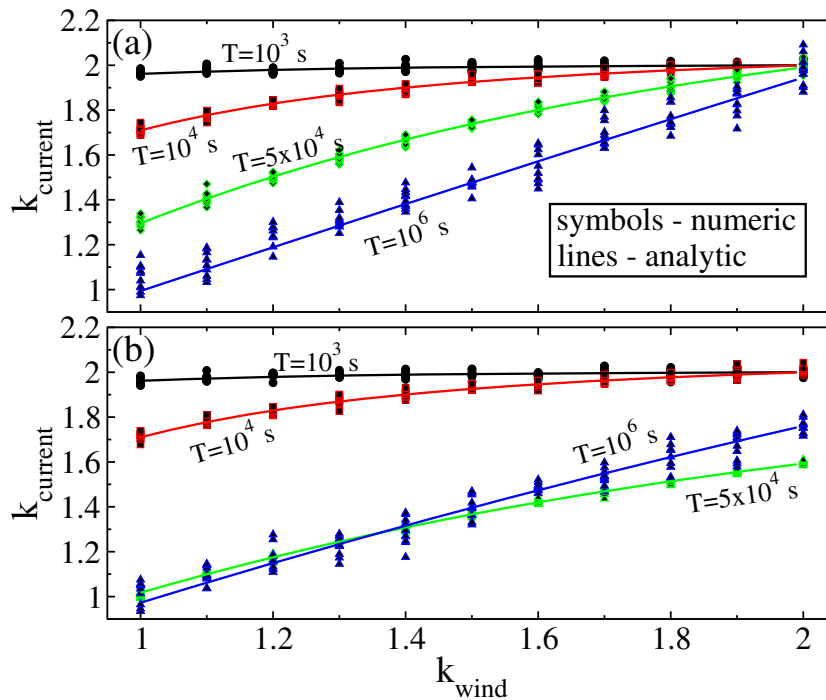
Figure 8. The Weibull $k_{current}$ parameter of the current distribution versus the k_{wind} parameter of the step-like wind-stress distribution. The analytical results (solid lines) are compared with the numerical solution of the Ekman model (symbols). The Coriolis parameter, f, in panel (a), is 0, corresponding to its value at the equator. In panel (b), $f \approx 1.45 \times 10^{-4}\,\text{s}^{-1}$, corresponding to its value at the pole and is larger than $r = 10^{-5}\,\text{s}^{-1}$. The different lines correspond to different constant wind-stress durations, T, as indicated in the figure.

are Gaussian-distributed independent random variables, then the distribution of $s = \sqrt{x^2 + y^2}$ is a Rayleigh distribution (a Weibull distribution with $k = 2$).

It is fairly easy to generate an uncorrelated Weibull-distributed time series (using a simple transformation rule). However, below we use time series that are both Weibull distributed and temporally correlated. Such time series are generated as follows:

(i)   Generate uncorrelated, Gaussian-distributed, time series.

(ii) Introduce temporal correlations by applying a Fourier transform to the time series from (i), multiply the obtained power spectrum by the power spectrum corresponding to the desired correlations (in our case, exponentially decaying temporal correlations) and apply an inverse Fourier transform.

(iii) Generate uncorrelated Weibull-distributed time series.

(iv) Rank order the time series from step (iii) according to the time series of step (ii).

The resulting time series is both temporally correlated and Weibull distributed. It is important to note that deviations from the desired Weibull parameters and the correlation time may occur due to the finite size of the time series. In order to minimize these deviations, one must ensure that the time series are much longer than the relevant correlation time. Elaborated
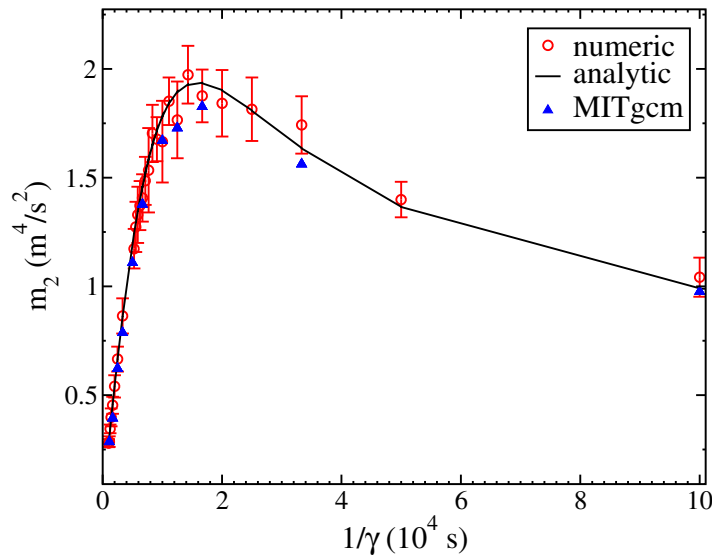
Figure 9. The second moment of the current amplitude for the case of wind stress with exponentially decaying temporal correlations. The analytical results (solid line) are compared with the results of numerical integration of Ekman equations (red circles) and with the currents simulated by the MITgcm model (blue triangles) in a simple lake with open boundaries (see the description in section 4). The red circles show the mean of different realizations of the wind stress in the numerical integration of the model and the bars show the standard deviation of these realizations. The wind-stress amplitude was drawn from a Weibull distribution with $k_{wind} = 1.5$. The Coriolis frequency, $f \approx 7.27 \times 10^{-5}\,\mathrm{s}^{-1}$, corresponds to its value at lat $= 30°$ and $r = 10^{-5}\,\mathrm{s}^{-1}$. Note that the second moment is plotted against $1/\gamma$, to allow easier comparison with the results of the step-like wind-stress case.

discussions of this and similar methods may be found in [22–24]. In deriving the results presented in the following section, we have used the algorithm mentioned above to generate the Weibull-distributed and temporally correlated wind stress. In addition, the parameters characterizing the Weibull distribution of the currents ($k_{current}$ and $\lambda_{current}$) were derived using the second and fourth moments and the relations mentioned in this subsection.

5. Results

The analytical results presented above for the idealized cases highlight the important role played by the temporal correlations of the wind stress in determining the statistics of surface ocean currents. The behaviors at the limits of long-range temporal correlations ($rT \gg 1$) and short-range temporal correlations ($T \to 0$) are intuitive, once derived. The existence of an optimal correlation time, at which the average current amplitude is maximal, is less trivial. A similar maximum was reported by Gonella [20], as described above. McWilliams and Huckle [25] (right panel of figure 11 of their paper) studied the Ekman layer rectification using the K-profile parameterization and observed a maximum in the depth-averaged variance of the
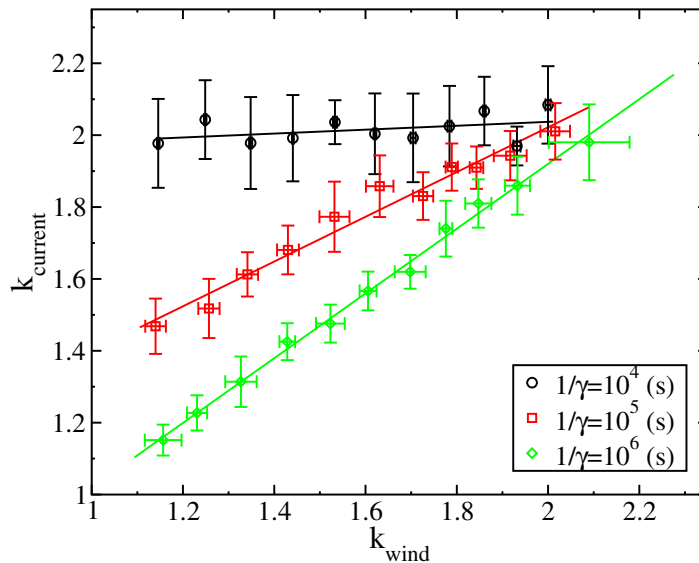
Figure 10. The Weibull $k_{current}$ parameter of the current amplitude distribution versus the k_{wind} parameter of the wind stress with exponentially decaying temporal correlations for different correlation times (corresponding to $1/\gamma$ as indicated in the figure). The results were obtained using different realizations of the wind stress. The symbols correspond to the mean and the bars to the standard deviation of the different realizations of the wind stress. Due to the finite size of the time series, there are also small deviations in the value of k_{wind}, and the horizontal bars show the standard deviation of these fluctuations. The solid lines are drawn to guide the eye. The values of the Coriolis parameter, f, and the Rayleigh friction parameter, r, are the same as in figure 9.

current speed as a function of the Markov memory time. In what follows, we present the results of the numerical tests.

In figure 6, we show the second moment of the current amplitude for the isotropic, step-like wind-stress model. The analytical results (equation (11)) are compared with the numerical solution of the Ekman model (equations (4)) and the MITgcm modeling of the currents in a simple artificial lake (details of which are provided above, using open boundaries with 1 km resolution). One can see that the dependence of the average current amplitude on the constant wind-stress duration is non-monotonic (due to the fact that the Coriolis effect is significant—$|f| > r$) and that there is excellent agreement between all the results. At the equator (not shown), where $f = 0$, the second moment increases monotonically to $\langle |\tau|^2 \rangle / (r^2 \rho_0^2)$ as a function of T.

It was previously argued that, under certain conditions, the wind amplitude (directly related to the wind stress) PDF is well approximated by the Weibull distribution [3]; we thus chose, in our demonstrations, a Weibull distribution of wind stress. In figure 7, we present the Weibull $k_{current}$ parameter (equation (16)) of the current distribution versus the constant wind-stress duration for two different values ($k_{wind} = 1$ and 2) of the wind-stress Weibull k_{wind} parameter (again, we only present here the results of the isotropic case). The analytical value of $k_{current}$ was found based on the ratio between the fourth moment and the square of the
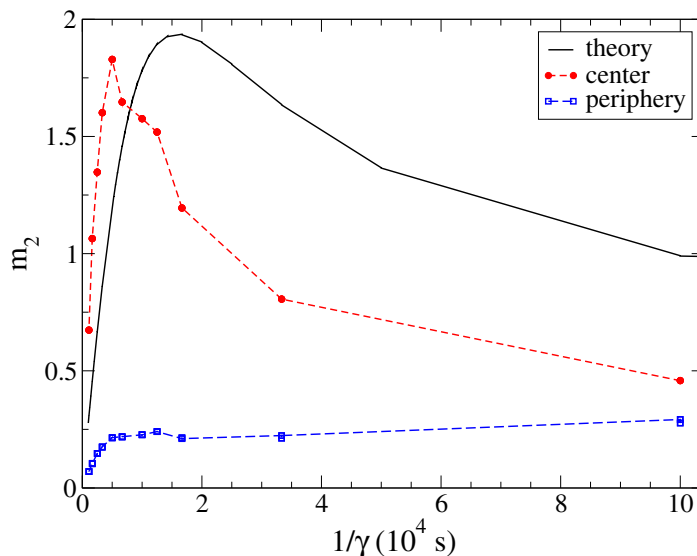
Figure 11. Comparison of the analytical results for the second moment of the current amplitude with the results of the detailed MITgcm model with closed boundaries and a coarse resolution of 10 km. It is shown that for a wide range of the wind-stress correlation times (the exponentially decaying temporal correlations were considered), the MITgcm results agree qualitatively with the analytical results of the over-simplified model. On the other hand, the results in the periphery show a significant deviation. These results, combined with the fact that for open boundaries, there was good agreement between the analytical and the simulations results, suggest that, as expected, the simple model fails to capture the boundary effects.

second moment; we note, however, that the current's PDF is not necessarily a Weibull PDF, and we chose to quantify the current's PDF using the k parameter of the Weibull distribution for presentation purposes only. The findings of [26] are consistent with the lower range of k_{wind} values used here. One can see that, for short correlation times, the current amplitude exhibits a Rayleigh distribution ($k_{current} = 2$), independent of the wind-stress distribution. This corresponds to Gaussian distributions of the current components. In the other limit of long constant wind-stress periods, $k_{current}$ converges to k_{wind} (not shown for $k_{wind} = 2$).

The above results were obtained for the maximal value of the Coriolis parameter, i.e. f at the pole. In figures 8(a) and (b), we show $k_{current}$ versus k_{wind} for different values of the constant wind-stress duration, T, and the two limiting values of the Coriolis parameter, f, at the equator and at the pole. Here again, one observes excellent agreement between the numerical and the analytical results for both values of f. The limits of short and long temporal correlations of the wind, at which $k_{current} = 2$ and $k_{current} = k_{wind}$, correspondingly, are clearly demonstrated.

In figures 9 and 10, we present similar results for the case of an exponentially decaying correlation function of the wind stress. As mentioned in section 3.2, the expression for the current's second moment (equation (15)) holds for any distribution of the wind stress (given that the temporal autocorrelation follows equation (13)), and thus it is possible to obtain analytically the current's second moment in the case of Weibull-distributed wind stress whose k value does

not necessarily equal 2. We generated a Weibull-distributed time series that has exponentially decaying temporal correlations, following the procedure described in section 4.2. In figure 9, we present the second moment of the current amplitude versus the correlation time (1/decay rate) of the correlation function. The existence of an optimal decay rate, for which the average current amplitude is maximal, is demonstrated for this case as well. One notable difference is the absence of the secondary maxima points which appeared in the step-like model. For this case, one may easily find that the maximal average amplitude of the currents is obtained for $\gamma = |f| - r$, assuming that $|f| \geqslant r$.

In figure 10, we present $k_{current}$ versus k_{wind}. Here again, we obtain excellent agreement between the predicted and the numerically obtained limiting behaviors. It is important to note that the good agreement between the MITgcm results and the analytical results has been proven to be valid only for the setup described above, using a fine resolution of 1 km and open boundaries. Different behaviors may occur for different scenarios, such as regions close to the boundary of the domain, spatially variable wind, complex and steep bottom topography, and vertically and spatially variable temperature and salinity. Using a setup with closed boundaries, we found that close to the boundaries of the artificial lake, the results showed a significant deviation due to the boundary effects that were neglected in the analytical model. The results of the MITgcm model with closed boundary conditions and coarser resolution of 10 km are shown in figure 11. All the other figures show the MITgcm results for the case of open boundaries. Moreover, we used a spatially uniform wind stress in our simulation and have not considered the more realistic case of non-uniform wind stress.

6. Summary

In summary, we have shown, in the two idealized cases, that the PDF of wind-driven ocean currents depends on the temporal correlations of the wind. For short-range correlations, the current speed approaches zero, and the PDF of its components is Gaussian. For long-range temporal correlations of the wind, the currents' PDF is proportional to the wind-stress PDF. The different cases considered here and the MITgcm simulations described above suggest that the existence of a maximal current speed as a function of the temporal correlation time is not unique for the cases studied here, and may also be relevant in more realistic types of temporal correlations and setups. An analysis that is based on the space-dependent model (either in the horizontal or the vertical dimensions or both) is a natural extension of the present study and will allow us to compare the analytical results to altimetry-based surface currents and to study non-local phenomena.

Acknowledgments

References

[1] Seguro J V and Lambert T W 2000 *Wind Eng. Ind. Aerodyn.* **85** 75–84
[2] Monahan A H 2006 *J. Clim.* **19** 497–520
[3] Monahan A H 2010 *J. Clim.* **23** 5151–62

IOP Institute of Physics **Φ** DEUTSCHE PHYSIKALISCHE GESELLSCHAFT

[4] Chu P C 2008 *Geophys. Res. Lett.* **35** L12606
[5] Gille S T and Smith S G L 1998 *Phys. Rev. Lett.* **81** 5249–52
[6] Gille S T and Smith S G L 2000 *J. Phys. Oceanogr.* **30** 125–36
[7] Chu P 2009 *J. IEEE Sel. Top. Appl. Earth Obs. Remote Sens.* **2** 27–32
[8] Ashkenazy Y and Gildor H 2011 *J. Phys. Oceanogr.* **41** 2295–306
[9] Ekman V W 1905 *Arch. Math. Astron. Phys.* **2** 1–52
[10] Gill A E 1982 *Atmosphere–Ocean Dynamics* (London: Academic)
[11] Cushman-Roisin B 1994 *Introduction to Geophysical Fluid Dynamics* 1st edn (Englewood Cliffs, NJ: Prentice-Hall)
[12] Airy G B 1845 On tides and waves *Encyclopedia Metropolitana* vol 5 (London: J J Griffin) pp 241–396
[13] Pollard R T and Millard R C 1970 *Deep Sea Res.* **17** 813–21
[14] Kundu P K 1976 *J. Phys. Oceanogr.* **6** 879–93
[15] Kase R H and Olbers D J 1979 *Deep Sea Res.* **26** 191–216
[16] Simons T J 1980 *Can. Bull. Fish. Aquat. Sci.* **203** 146
[17] van Kampen N G 1981 *Stochastic Processes in Physics and Chemistry* (Amsterdam: North-Holland)
[18] Monahan A H 2007 *J. Clim.* **20** 5798–814
[19] Monahan A H 2012 *J. Clim.* **25** 6684–700
[20] Gonella J 1971 *Deep Sea Res.* **18** 775–88
[21] MITgcm Group 2010 *MITgcm User Manual* (Cambridge, MA: MIT/EAPS) http://mitgcm.org/public/r2_manual/latest/online_documents/manual.html
[22] Schreiber T and Schmitz A 1996 *Phys. Rev. Lett.* **77** 635
[23] Schreiber T and Schmitz A 2000 *Physica* D **142** 346
[24] Kantz H and Schreiber T 2004 *Nonlinear Time Series Analysis* (Cambridge: Cambridge University Press)
[25] McWilliams J C and Huckle E 2005 *J. Phys. Oceanogr.* **36** 1646–59
[26] Monahan A H 2008 *Geophys. Res. Lett.* **35** L05704
[27] Kalnay E *et al* 1996 *Bull. Am. Meteorol. Soc.* **77** 437–71